PAPER

Check for updates

Secondary ligand-induced orthogonal self-assembly of silver nanoclusters into superstructures with enhanced NIR emission†

Korath Shivan Sugi, [ID] [a,b] Amritha P. Sandra, [ID] [a,b] Nonappa, [ID] [c] Debasmita Ghosh,[a,b] Jyoti Sarita Mohanty,[a,b] Murugesan Paulthangam Kannan, [ID] [a,b] B. S. Sooraj, [ID] [a,b] Pillalamarri Srikrishnarka, [ID] [a,b] Jyoti Roy,[a,b] Wakeel Ahmed Dar[a,b] and Thalappil Pradeep [ID] *[a,b]

Orthogonal self-assembly is one of the crucial strategies for forming complex and hierarchical structures in biological systems. However, creating such ordered complex structures using synthetic nanoparticles is a challenging task and requires a high degree of control over structure and multiple non-covalent interactions. In this context, nanoarchitectonics serves as an emerging tool to fabricate complex functional materials. Here, we present a secondary ligand-induced orthogonal self-assembly of atomically precise silver nanoclusters into complex superstructures. Specifically, we use $Ag_{14}NCs$ protected with naphthalene thiol and 1,6-bis(diphenylphosphino)hexane ligands. Controlled addition of 1,6-bis(diphenylphosphino)hexane, the secondary ligand resulted in a self-assembled supracolloidal structure including helical fibers, spheres, and nanosheets. The self-assembly process is tunable by controlling the molar ratio of the ligand. The resulting superstructures exhibit enhanced NIR emission due to restricted intramolecular motion. This demonstrates that by tuning supramolecular interactions, hierarchical nanostructures with desired properties similar to biomolecules can be obtained from atomically precise building blocks.

[a]*DST Unit of Nanoscience (DST UNS) and Thematic Unit of Excellence (TUE), Department of Chemistry, Indian Institute of Technology Madras, Chennai 600 036, India. E-mail: pradeep@iitm.ac.in*
[b]*International Centre for Clean Water, Chennai 600113, India*
[c]*Faculty of Engineering and Natural Sciences, Tampere University, FI-33720 Tampere, Finland*

†Electronic supplementary information (ESI) available: Collision-induced dissociation mass spectra, SEM image and EDS mapping, XPS, ^{31}P NMR of Ag_{14} nanoclusters, TEM images showing the structural evolution of Ag_{14} nanoclusters with the addition of different molar ratios of DPPH ligands, TEM images of NCA-1.0, STEM images of NCA-1.0, UV-vis spectrum and ESI MS of NCA-1.0 redispersed in DMF, TEM images of the DPPH-NT mixture, and schematic illustration of supramolecular interactions in Ag_{14} nanoclusters. See DOI: https://doi.org/10.1039/d3nr02561f

Introduction

Self-assembly of molecular building units into complex functional and structural biological superstructures is omnipresent in nature.[1–3] Orthogonal self-assembly is one of the important features of biological systems.[4–8] In orthogonal self-assembly, multiple but non-interfering non-covalent interactions play a crucial role in the formation of complex structures. Examples include the double helical structure of DNA, protein folding, and cell membranes.[2,3,9] Extensive research has been conducted to synthesize/mimic such biological architectures using molecular-level building blocks, supramolecular polymers, and metal–ligand complexes using orthogonal self-assembly.[6,7,10–13] Hierarchical structures of metallacycles and metallacages are fabricated by exploiting the orthogonal metal–ligand coordination and other noncovalent interactions.[9] Sun *et al.* demonstrated that alanine-based chiral metallacycles could self-assemble into nanospheres at low concentrations and chiral metallogels at high concentrations utilizing the noncovalent interactions.[12] Recently, nano architectures from nanomaterials are fabricated using the nanoarchitectonics concept.[14–16]

Despite numerous efforts using molecular and macromolecular building blocks, orthogonal self-assembly of synthetic metal nanoparticles has been a challenge. This is attributed to non-uniform size, uncontrolled ligand density, and aggregation tendencies. In recent years, atomically precise metal nanoclusters (NCs)[17,18] have gained attention as functional materials due to their small size, well-defined structure, and unique physical properties.[19] They are considered as potential luminophores due to their unique optical properties.[20,21] They are also known to self-assemble into hierarchical structures reminiscent of biological systems.[22,23] Several strategies are employed to assemble NCs into dimers and higher hierarchi-

cal structures, which show self-assembly-induced luminescence, mechanical performance, and biological activities.[22,24–27] The most common strategies involve the functionalization of protecting ligands and introducing new linkers such as organic molecules, ions, counterions, solvents, and phase transfer agents that can induce self-assembly in NCs.[28,29] Well-defined cluster assembled solids (CASs) have been assembled by exploiting the noncovalent interactions-mediated inter-cluster assembly.[30] Apart from their ease of handling, hierarchical/supramolecular architectures of atomically precise NCs retain the intrinsic properties of individual NCs and at the same time display emerging or collective properties.[31,32]

In this context, a facile and novel route is demonstrated here to self-assemble NCs into supramolecular architectures reminiscent of biomolecules. We have synthesized Ag_{14} nanoclusters co-protected by naphthalene thiolate and 1,6-bis(diphenylphosphino)hexane (DPPH). These NCs exhibited distinct optical properties compared to analogous Ag_{14} NCs protected with different ligands.[33–36] By controlled addition of DPPH as a bidentate secondary ligand, the Ag_{14} NCs initially assemble into thin sheets. The sheets further assemble into spherical superstructures and rope-like wraps. Mass spectrometric investigations of supramolecular structures reveal the formation of NC-DPPH adducts. Such supramolecular architectures of NCs show enhanced near-infrared (NIR) emission due to the restricted intramolecular motion (RIM). We believe that such assemblies are directed by the supramolecular interactions between bidentate DPPH ligands and naphthalene thiol (NT) ligands, also the long chain of DPPH acts as a bridge between two NCs resulting in an orthogonal assembly. This method could pave the way to create hierarchical NC architectures with desired properties, which can further offer new avenues to programmable self-assembly of NCs with controllable properties.

Experimental section

Materials

Silver nitrate ($AgNO_3$) was purchased from RANKEM. 1-Napthalenethiol (NT), 1,6-bis(diphenylphosphino)hexane (DPPH), tetraphenylphosphonium chloride (PPh_4Cl), triethylamine (TEA), and sodium borohydride ($NaBH_4$) were purchased from Sigma Aldrich. All other solvents such as methanol, hexane, dichloromethane (DCM), trichloromethane (TCM), and *N,N*-dimethylformamide (DMF) were of analytical grade.

Characterization

PerkinElmer Lambda 25 spectrometer was used to record the UV-Vis absorption spectrum of the nanocluster samples. Photoluminescence measurements were carried out using a Horiba Jobin Yvon NanoLog instrument. Mass spectrometric measurements were performed using a Waters Synapt G2 Si instrument (details in ESI†). The X-ray photoelectron spectroscopy (XPS) measurements of nanocluster samples were carried out with an Omicron ESCA Probe Spectrometer. Nuclear magnetic resonance (NMR) spectra (^{31}P) of the nanocluster samples were recorded using a 500 MHz Bruker Avance III spectrometer. Dynamic light scattering (DLS) measurements were performed using a Malvern Zetasizer ZSP instrument. High-resolution transmission electron microscopy (HRTEM) was performed with a JEOL 3010. Scanning electron microscope (SEM) images and energy dispersive X-ray analysis (EDAX) were collected using an FEI QUANTA-200 SEM. Scanning transmission electron microscope (STEM) imaging was performed using JEOL JEM-2800 high throughput electron microscope equipped with a Schottky type field emission gun operated at 200 kV with simultaneous bright field (BF) and dark field (DF) STEM imaging. For elemental mapping energy dispersive X-ray mapping and spectra were collected using dual silicon drift detectors. The tilt series for electron tomographic reconstruction of the nanocluster assembled architectures were collected using the JEM 3200FSC microscope operated at 300 keV (see electronic ESI† for details).

Synthesis of $Ag_{14}(NT)_7(DPPH)_2Cl_2$ nanoclusters

The $Ag_{14}(NT)_7(DPPH)_2Cl_2$ NCs were synthesized by dissolving 20 mg of silver nitrate in 3 mL of methanol. To this solution, 11 mL of DCM was added. A 10 μL of 1-NT was added and the reaction is carried out at 0 °C. After the addition of NT, the color of the solution changed to turbid yellow indicating the formation of silver thiolates. After 5 minutes, 6.8 mg of DPPH (in 0.5 mL DCM) and 6 mg of PPh_4Cl (in 0.5 mL DCM) were added. After 30 minutes, 45 mg of $NaBH_4$ in 1 mL ice-cold (DI) water and 50 μL of TEA were added. The color of the solution changed to dark brown after the addition of $NaBH_4$. After five hours of continuous stirring, the crude cluster was kept in the fridge overnight for size focusing. The resultant material was centrifuged and the precipitate was washed several times with methanol, hexane, and DMF and dispersed in DCM or TCM for characterization.

Secondary ligand-induced nanoarchitectures of Ag_{14} nanoclusters

Approximately 10 mg of $Ag_{14}(NT)_7(DPPH)_2Cl_2$ NCs were dissolved in 10 mL of TCM. To this NC solution, the DPPH ligand was added with the molar ratio of DPPH/NC ranging from 0.5 to 10.

Results and discussion

Characterization of Ag_{14} nanoclusters

Naphthalene thiol-protected Ag_{14}NCs were synthesized and characterized according to the methods described in the experimental section. The quantized electronic structure of the NCs is evident from the optical absorption spectral peaks centered at 340, 490, and 690 nm (Fig. 1A). They also display intense NIR emission at 1035 nm when excited at 340 nm (inset of Fig. 1A). The ESI MS in the positive mode resulted in a peak centered at *m/z* 3605, which was assigned as $[Ag_{14}(NT)_7(DPPH)_2Cl_2]$ (Fig. 1B). Experimental and theoretical
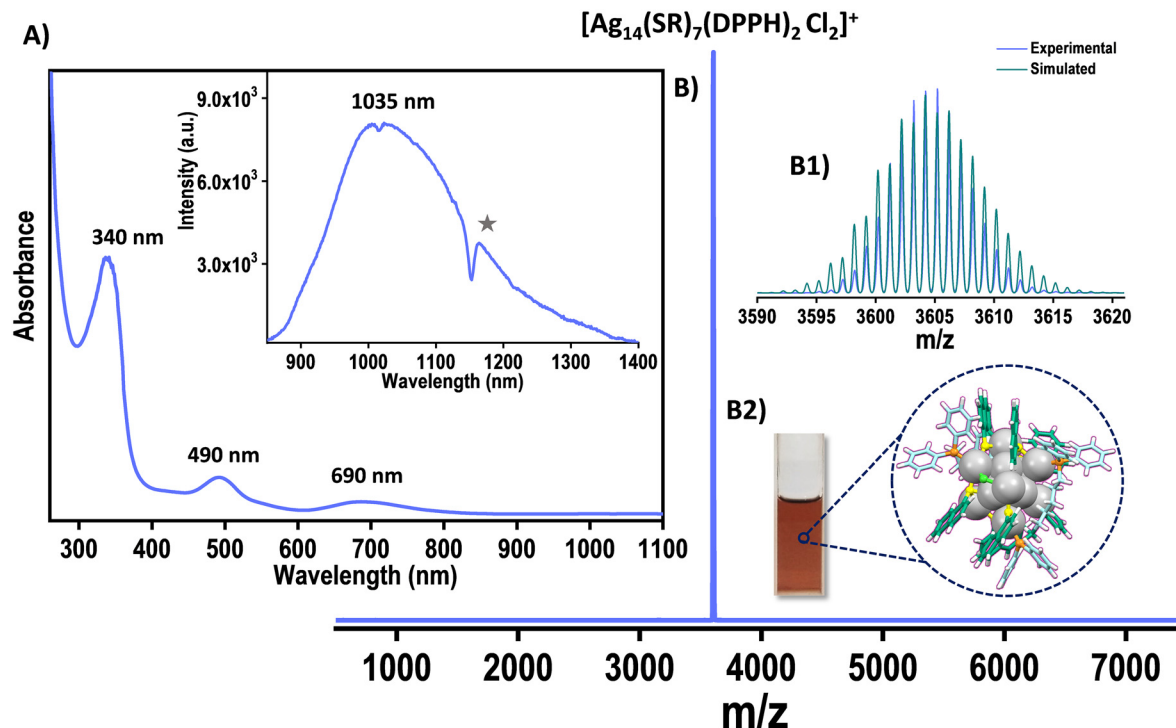
Fig. 1 (A) UV-Vis spectrum of Ag_{14} NCs. Inset of A shows the emission at 340 nm excitation of Ag_{14} NCs (star symbol (*) denotes the solvent-induced structuration).[37] (B) The ESI MS of Ag_{14} NCs. (B1) The experimental and simulated spectra match well. (B2) Photograph of the Ag_{14} NC solution. Color codes: grey, Ag; blue/sea green, C; yellow, S; orange, P; green, Cl; white, H.

isotopic distribution matched well and revealed that the Ag_{14} NCs are monovalent (Fig. 1B1).

Collision-induced dissociation (CID) study of $[Ag_{14}(NT)_7(DPPH)_2Cl_2]^+$ further reaffirms the assigned molecular formula (Fig. S1†). A systematic loss of DPPH and NT ligand (L) was observed with an increase in collision energy (CE). Initially, one DPPH was lost, and with further increase in the CE, the second DPPH unit was lost, followed by other primary ligands. The composition of Ag_{14} NC was further confirmed by elemental analysis which confirms the presence of Ag, S, Cl, and P. Their atomic percentages matched well with the assigned formula (Fig. S2†). Besides, elemental characterization was also performed using X-ray photoelectron spectroscopy (XPS). Peaks corresponding to Ag $3d_{5/2}$, S $2p_{3/2}$, P $2p_{3/2}$, and Cl $2p_{3/2}$ appeared at ~368.5, ~162.9, ~131.8, and ~198.3 eV, respectively (Fig. S3†).

The ^{31}P NMR spectrum of DPPH alone shows major signals at 32.7 and −17.1 ppm (Fig. S4†), which can be attributed to oxidized species such as $DPPHO_2$ and uncoordinated DPPH ligands.[38] The ^{31}P NMR spectrum of Ag_{14} NCs shows two doublets due to the coupling of ^{31}P with ^{109}Ag and ^{107}Ag, which implies the coordination of the DPPH ligand to silver.[39,40]

Ligand engineering induced tailoring of the optical properties

The UV-vis spectrum of the NT-protected Ag_{14} NCs is compared with that of the other two Ag_{14} NCs reported in the literature.[33,34] A drastic change in optical properties was

observed for NT-protected Ag_{14}NCs (Fig. 2). The UV-vis spectrum of $Ag_{14}(3,4\text{-DFBT})_{12}TPP_8$ (3,4-DFBT = 3,4 difluorobenzenethiol, TPP = triphenylphosphine) displays two major absorption bands at 368 and 530 nm whereas, $Ag_{14}(1,2\text{-BDT})_6TPP_8$ (1,2-BDT = 1,2 benzenedithiol, TPP = triphenylphosphine) shows peaks at 425, 600, and 860 nm. The $[Ag_{14}(NT)_7(DPPH)_2Cl_2]$ NC shows molecular peaks at 340, 490, and 690 nm. The $Ag_{14}(3,4\text{-DFBT})_{12}TPP_8$ NCs display dual emis-

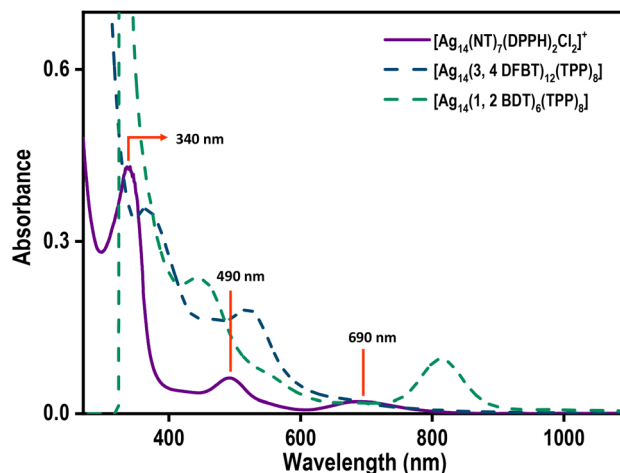**Fig. 2** The UV-vis spectra of $[Ag_{14}(NT)_7(DPPH)_2Cl_2]^+$ (violet trace), $Ag_{14}(3,4\ DFBT)_{12}TPP_8$ (dark blue trace), and $Ag_{14}(1,2\ BDT)_6TPP_8$ (sea green trace).

sion peaks around 536 nm and 420 nm. Such dual emission was also observed in the case of $Ag_{14}(1,2\text{-BDT})_6TPP_8$ NCs. The NT-protected Ag_{14} NCs, in contrast, show NIR emission at 1035 nm. This observation signifies the pivotal role of ligands in tailoring the optoelectronic properties of NCs.

Secondary ligand-induced assembly of Ag_{14} NCs

NCs are assembled into hierarchical structures using strategies that involve introducing organic molecules, ions, counterions, solvents, and phase transfer agents. The secondary ligand induced transformation and self-assembly of nanoclusters are studied in detail.[41–43] Considering the long-chain length of the bidentate DPPH ligand, we were motivated to introduce different ratios of DPPH ligands to induce self-assembly in Ag_{14} NCs.

Different concentrations of DPPH were introduced into the Ag_{14} NCs, and their corresponding UV-vis spectra were monitored (Fig. 3). The resulting NC architectures (NCA) are labelled as NCA-0.5, NCA-1.0, NCA-3.0, NCA-5.0, and NCA-10.0 with 0.5, 1.0, 3.0, 5.0, and 10.0 mole ratio of DPPH (with respect to the cluster), respectively. Up to a 1.0 mole ratio, the molecular features of Ag_{14} NCs were intact, with further increasing the concentration of DPPH, the NC solution becomes colorless. The corresponding UV-vis spectrum reveals the disappearance of major molecular features centered at 490 and 690 nm of the NCs. The peak at 340 nm is red shifted to 390 nm. We assume that this could be due to the degradation of NCs. The disappearance of NC features with increased DPPH ligands concentration illustrates that the NCs decompose or transform in this operation. The TEM images of Ag_{14} NCs with different concentrations of DPPH revealed the formation of supramolecular hierarchical structures (Fig. S5†). The NCA-0.5 shows a sheet-like assembly, and NCA-1.0 forms right-handed (P-type) super-helical bundles (Fig. S6 and S7†) or coiled coil-like structures[44,45] alongside spherical structures

Fig. 3 Variation of UV-vis spectra trend of $[Ag_{14}(NT)_7(DPPH)_2Cl_2]^+$ NCs with the addition of different mole ratios of DPPH ligand. Inset shows the corresponding photographs of the NCs solutions.

of ~200–300 nm (Fig. S8†). The EDS mapping of NCA 1.0 shows the presence of Ag, S, Cl, P and C which further suggests the aggregation of NCs (Fig. S9, S10, and S11†). With further increase in the concentration of DPPH, we have observed sheets and aggregates, which could be due to the decomposition or transformation of NCs; as also evident from the ^{31}P NMR data (Fig. S12 and S13†). The NCA-1.0 was analyzed in greater detail. The magnified images of spheres and helical bundles, similar to intermediate filaments such as keratin suggest that they comprise atomically precise Ag_{14} NCs (Fig. 4). Resolving the three-dimensional (3D) structures using electron tomography (ET) reconstruction reaffirms the spherical nature of superstructures (Fig. 4D and E). The cross-sectional view of the sphere reveals a solid interior due to the Ag_{14} NC assembly (Fig. 4F). Such NC assemblies could be formed by the inter-cluster supramolecular interactions between the NT ligands and secondary DPPH ligands.

Dynamic light scattering (DLS) studies unveil the size evolution of the nanostructures formed during the controlled addition of DPPH ligands (Fig. 4G). The average size of Ag_{14} NCs was found to be 3.2 ± 0.36 nm; NCA-0.5 shows an average size of 245 ± 2 nm. The NCA-1.0 superstructures show an average size of 375 ± 5 nm. With further increasing the concentration of DPPH, the size reduces, suggesting small aggregates and dissolved species.

To gain more insight into the NC assembled super-structures, we have performed ESI MS. Along with the parent NC ion (X^+), several new peaks were observed in the ESI MS of NCA-1.0 in the m/z range of 3900–4600 (Fig. 5). Detailed analysis of the peaks reveals that they are NC-DPPH adducts, the composition of the adducts are $[X_3Y_3]^{3+}$ (Y = DPPH), (m/z 4059), $[X_2Y_3]^{2+}$ (m/z 4287) along with other fragmentation peaks (Fig. 5). Higher NC-DPPH adducts were not observed, which could be due to their lower ionization efficiency. The compositions and the charge states of the adducts were determined by analyzing the m/z values and isotopic patterns of the peaks. In the isotopic distribution of $[X_3Y_3]^{3+}$, the difference between the peaks is m/z 0.33, which confirmed a charge state of 3+ (Fig. 5A2). The experimental isotopic distribution matches well with the theoretical isotopic distribution of $[X_3Y_3]^{3+}$, which further reaffirms the assigned composition. The difference between peaks in the isotopic distribution of $[X_2Y_3]^{2+}$ is m/z 0.5, which suggests a charge state of 2+ (Fig. 5A3). Along with these adducts there are several other low intensity peaks which could be due to weak gas phase adducts of X and Y. Due to low intensity, we could not perform CID measurements on the DPPH-mediated trimers and dimers of Ag_{14} NCs. To understand the role of DPPH in directing the hierarchical structures, NCA-1.0 was redispersed in DMF as DPPH is insoluble in DMF and analysed using UV-vis spectroscopy and ESI MS (Fig. S14†). The ESI MS in DMF didn't show any NC adducts which further confirms the role of DPPH in the NC assembly (Fig. S14†). We have also performed TEM measurements of the DPPH–NT mixture, which revealed that they also form thin sheets (Fig. S15†). The formation of sheet-like structures further reaffirms the supramolecular inter-
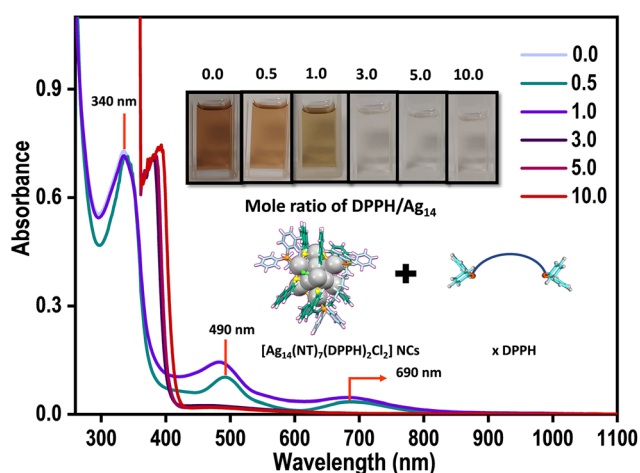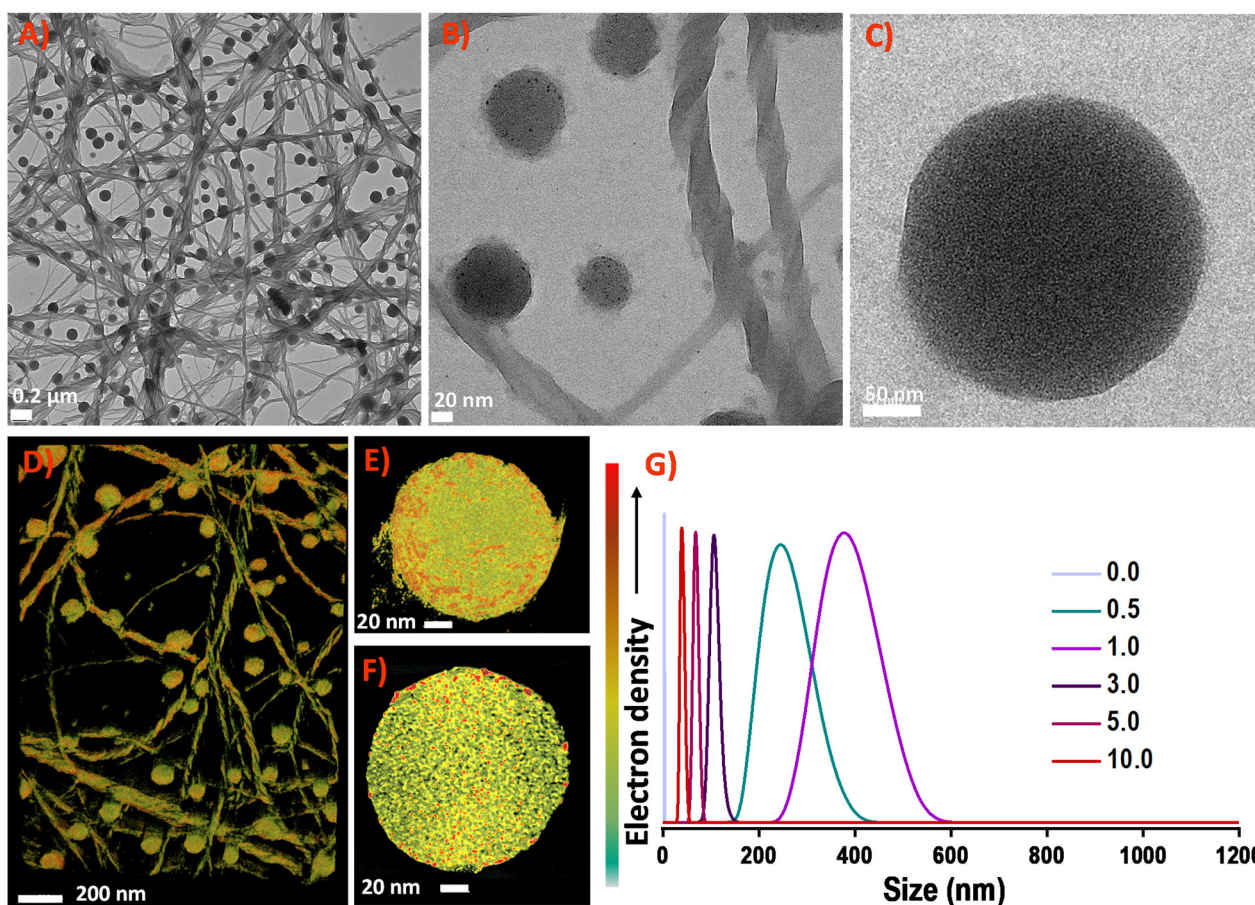
Fig. 4 TEM images showing the self-assembled superhelices and spheres NCA-1.0. Magnified TEM images are shown in A–C. (D) Electron tomography (ET) reconstruction of NCA-1.0. (E) and (F) are the 3D reconstructed structure of the Ag_{14} NC assembled sphere and its cross-sectional view. (G) DLS measurements show variation in size of $[Ag_{14}(NT)_7(DPPH)_2Cl_2]^+$ NCs with the addition of different molar ratios of DPPH ligands.
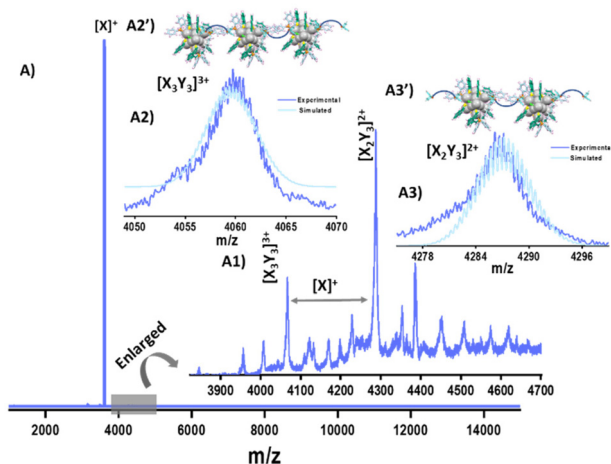

Fig. 5 (A) ESI MS showing the supramolecular adducts in NCA-1.0. (A1) Enlarged view of the same. (A2) The experimental and theoretical isotopic patterns of $[X_3Y_3]^{3+}$. (A2') Schematic representation of $[X_3Y_3]^{3+}$. (A3) The experimental and theoretical isotopic patterns of $[X_2Y_3]^{2+}$. (A3') Schematic representation of $[X_3Y_3]^{2+}$. (X = $[Ag_{14}(NT)_7(DPPH)_2Cl_2]$; Y = DPPH). Color codes: grey, Ag; blue/sea green, C; yellow, S; orange, P; green, Cl; white, H.

actions between the primary NT ligands and secondary DPPH ligands.

Mechanism for the formation of supramolecular architectures

We speculate that the optimum concentration of DPPH directs orthogonal self-assembly, which leads to the formation of two different supramolecular architectures in the same system. Specific non-covalent intermolecular interactions could direct the formation of such interpenetrating networks. Orthogonal self-assembly[6,11,13] is an essential strategy in biological systems, where complex structures are generated by highly specific non-covalent interactions between constituents such as proteins, amphiphiles, and biopolymers.[10] In supramolecular chemistry, specific non-covalent interactions are exploited to achieve such orthogonal self-assembly.[46] The naphthalene diimide chromophores[47] are known to organize into supramolecular helices.[48] Substitutions on naphthalene had resulted in helical tubes,[49] twisted ribbons or helices with preferred handedness.[50]

Based on microscopic and spectroscopic investigations, we propose that the orthogonal self-assembly process of Ag_{14} NCs

relies on (i) bidentate nature of DPPH ligand, (ii) $\pi\cdots\pi$ stacking of the NT ligands in Ag_{14} NCs, (iii) $CH\cdots\pi$ interactions between NT and DPPH ligands (Fig. S16†), and (iv) $H\cdots H$ interactions between NT ligands (Scheme 1). Such covalent and non-covalent interactions together lead to the formation of the microspheres and sheets/films of Ag_{14} NCs (Scheme 1A1) whereas, a lower degree of self-assembly in the z-axis results in the formation of superhelices which tends to bundle to form rope-like NC assemblies (Scheme 1A2). Compared to other ligand-protected Ag_{14} nanoclusters such as $Ag_{14}(3,4\text{-DFBT})_{12}TPP_8$,[34] $Ag_{14}(1,2\text{-BDT})_6TPP_8$[33] and $Ag_{14}(pntp)_{10}(dpph)_4Cl_2$,[51] $[Ag_{14}(NT)_7(DPPH)_2Cl_2]^+$ NCs are ligand deficient. Therefore, their surface structure can afford a few more ligands without stripping the thiolates and phosphines. The NT and DPPH ligands and their $\pi\cdots\pi$ and $CH\cdots\pi$ interactions play a crucial role in directing such orthogonal self-assembled nanostructures.

Enhanced emission

The optical features of Ag_{14} NCs were retained up to NCA-1.0 which suggests that the NC property is retained in hierarchical structures. This prompted us to investigate their emission properties. A significant enhancement in the emission of Ag_{14} NCs assembled superstructures was observed (Fig. 6).

A three-fold enhancement in PL emission was observed in the case of NCA-1.0 than its parent Ag_{14} NCs. With increasing the concentration of DPPH (3.0, 5.0, and 10.0), the PL intensity reduces significantly. Increment in the emission of Ag_{14} NCs in solution by the addition of DPPH is attributed to the restricted motion of the ligands through ordered self-assembly. Atomically precise NCs are known to display aggregation-induced emission (AIE) due to restrictions in the intermolecular rotation (RIR).[52] The ordered assembly of surface motifs in aggregation-induced nanostructures reduces vibrational relaxation enhancing emission.[53] The inter-nanocluster $CH\cdots\pi$ interactions are also known to restrict the intramolecular rotations/vibrations and amplify the PL emission of NCs.[54] We hypothesize that inter-nanocluster $CH\cdots\pi$ and $\pi\cdots\pi$
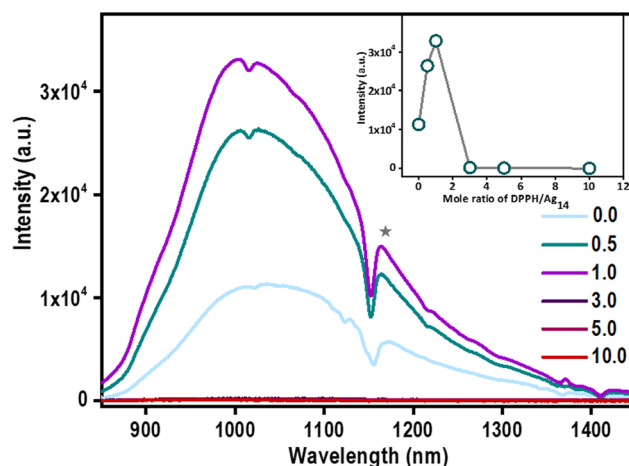

Fig. 6 Variation of PL trend of $[Ag_{14}(NT)_7(DPPH)_2Cl_2]^+$ NCs with the addition of different mole ratios of DPPH ligand (the star denotes the solvent-induced structuration). Inset shows the variation of PL intensity at 1035 nm with a different mole ratio of DPPH ligand.

interactions that direct the ordered assembly of the NCs together restrict the molecular rotations and enhances the emission.

Conclusions

In this work, we demonstrate a novel facile route for creating supramolecular architectures of atomically precise NCs. The controlled addition of bidentate secondary ligand DPPH directs the orthogonal self-assembly of NCs reminiscent of biological systems. The mass spectrometric investigations reveal that the supramolecular architectures are formed by the assembly of NC–DPPH adducts. The distinct non-covalent interactions of surface motifs with excess secondary bidentate ligands play a pivotal role in such orthogonal self-assembly of NCs. The self-assembled structures show an enhanced NIR emission due to restricted intramolecular motion (RIM). To the best of our knowledge, this is the first example of secondary-ligand induced orthogonal self-assembly of atomically precise NCs. We envision the application of orthogonal self-assembly approaches to create self-assembled structures from atomically precise NCs that offer complex hierarchical architectures of NCs.

Author contributions

K.S.S and A.P.S performed synthesis, and other experimental studies. Nonappa performed electron tomography, HRTEM and STEM studies. D.G and J.R performed mass spectrometric studies. J.S.M performed the TEM measurements. M.P.K performed XPS studies. B.S.S performed NMR studies. P.S performed SEM measurements. W.A.D was involved in the discussion of experimental data. K.S.S wrote the first draft of the manuscript and all co-authors have given approval to the final
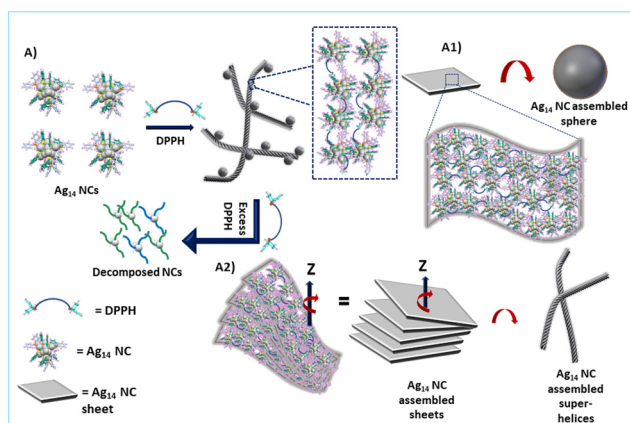
Scheme 1 Schematic illustration showing the mechanism of DPPH-induced orthogonal self-assembly of Ag_{14} NCs into superhelices and spheres.

version of the manuscript. T.P conceptualized and finalized the manuscript.

Conflicts of interest

There are no conflicts to declare.

Acknowledgements

References

1 J. D. Watson and F. H. C. Crick, *Nature*, 1953, **171**, 737–738.
2 T. Xiao, X.-Q. Sun and L. Wang, in *Handbook of Macrocyclic Supramolecular Assembly*, ed. Y. Liu, Y. Chen and H.-Y. Zhang, Springer Singapore, Singapore, 2019, pp. 1–28, DOI: 10.1007/978-981-13-1744-6_54-1.
3 T. Leigh and P. Fernandez-Trillo, *Nat. Rev. Chem.*, 2020, **4**, 291–310.
4 C. K. McLaughlin, G. D. Hamblin and H. F. Sleiman, *Chem. Soc. Rev.*, 2011, **40**, 5647–5656.
5 P. Yakovchuk, E. Protozanova and M. D. Frank-Kamenetskii, *Nucleic Acids Res.*, 2006, **34**, 564–574.
6 M. L. Saha, S. De, S. Pramanik and M. Schmittel, *Chem. Soc. Rev.*, 2013, **42**, 6860–6909.
7 X.-Y. Hu, T. Xiao, C. Lin, F. Huang and L. Wang, *Acc. Chem. Res.*, 2014, **47**, 2041–2051.
8 T. Xiao, X.-Q. Sun and L. Wang, *Handbook of Macrocyclic Supramolecular Assembly*, 2020, pp. 1317–1344.
9 S. Datta, M. L. Saha and P. J. Stang, *Acc. Chem. Res.*, 2018, **51**, 2047–2063.
10 J. Boekhoven, A. M. Brizard, M. C. A. Stuart, L. Florusse, G. Raffy, A. Del Guerzo and J. H. van Esch, *Chem. Sci.*, 2016, **7**, 6021–6031.
11 P. Wei, X. Yan and F. Huang, *Chem. Soc. Rev.*, 2015, **44**, 815–832.
12 Y. Sun, S. Li, Z. Zhou, M. L. Saha, S. Datta, M. Zhang, X. Yan, D. Tian, H. Wang, L. Wang, X. Li, M. Liu, H. Li and P. J. Stang, *J. Am. Chem. Soc.*, 2018, **140**, 3257–3263.
13 S. Datta, S. K. Misra, M. L. Saha, N. Lahiri, J. Louie, D. Pan and P. J. Stang, *Proc. Natl. Acad. Sci. U. S. A.*, 2018, **115**, 8087–8092.
14 K. Ariga, T. Mori, T. Kitao and T. Uemura, *Adv. Mater.*, 2020, **32**, 1905657.
15 V. Karthick, L. Kumar Shrestha, V. G. Kumar, P. Pranjali, D. Kumar, A. Pal and K. Ariga, *Nanoscale*, 2022, **14**(30), 10630–10647.
16 K. Ariga, *Nanoscale*, 2022, **14**(30), 10610–10629.
17 R. Jin, C. Zeng, M. Zhou and Y. Chen, *Chem. Rev.*, 2016, **116**, 10346–10413.
18 I. Chakraborty and T. Pradeep, *Chem. Rev.*, 2017, **117**, 8208–8271.
19 J. V. Rival, P. Mymoona, K. M. Lakshmi, Nonappa, T. Pradeep and E. S. Shibu, *Small*, 2021, **17**, 2005718.
20 H. Zhang, Z. Zhao, P. R. McGonigal, R. Ye, S. Liu, J. W. Y. Lam, R. T. K. Kwok, W. Z. Yuan, J. Xie, A. L. Rogach and B. Z. Tang, *Mater. Today*, 2020, **32**, 275–292.
21 Nonappa, *Beilstein J. Nanotechnol.*, 2020, **11**, 533–546.
22 C. Zeng, Y. Chen, K. Kirschbaum, K. J. Lambright and R. Jin, *Science*, 2016, **354**, 1580–1584.
23 Y. Li, M. Zhou, Y. Song, T. Higaki, H. Wang and R. Jin, *Nature*, 2021, **594**, 380–384.
24 Q. Li, J. C. Russell, T.-Y. Luo, X. Roy, N. L. Rosi, Y. Zhu and R. Jin, *Nat. Commun.*, 2018, **9**, 3871.
25 S. Chandra, Nonappa, G. Beaune, A. Som, S. Zhou, J. Lahtinen, H. Jiang, J. V. I. Timonen, O. Ikkala and R. H. A. Ras, *Adv. Opt. Mater.*, 2019, **7**, 1900620.
26 Y. Bi, Z. Wang, T. Liu, D. Sun, N. Godbert, H. Li, J. Hao and X. Xin, *ACS Nano*, 2021, **15**, 15910–15919.
27 J. Shen, Q. Xiao, P. Sun, J. Feng, X. Xin, Y. Yu and W. Qi, *ACS Nano*, 2021, **15**, 4947–4955.
28 A. Ebina, S. Hossain, H. Horihata, S. Ozaki, S. Kato, T. Kawawaki and Y. Negishi, *Nanomaterials*, 2020, **10**, 1105.
29 Z. Wu, Q. Yao, S. Zang and J. Xie, *ACS Mater. Lett.*, 2019, **1**, 237–248.
30 X. Kang and M. Zhu, *Coord. Chem. Rev.*, 2019, **394**, 1–38.
31 A. Som, A. Griffo, I. Chakraborty, H. Hähl, B. Mondal, A. Chakraborty, K. Jacobs, P. Laaksonen, O. Ikkala, T. Pradeep and Nonappa, *Small*, 2022, **18**, 2201707.
32 P. Sun, Z. Wang, Y. Bi, D. Sun, T. Zhao, F. Zhao, W. Wang and X. Xin, *ACS Appl. Nano Mater.*, 2020, **3**, 2038–2046.
33 M. Bodiuzzaman, E. Khatun, K. S. Sugi, G. Paramasivam, W. A. Dar, S. Antharjanam and T. Pradeep, *J. Phys. Chem. C*, 2020, **124**, 23426–23432.
34 H. Yang, J. Lei, B. Wu, Y. Wang, M. Zhou, A. Xia, L. Zheng and N. Zheng, *Chem. Commun.*, 2013, **49**, 300–302.
35 A. Jana, M. Jash, A. K. Poonia, G. Paramasivam, M. R. Islam, P. Chakraborty, S. Antharjanam, J. Machacek, S. Ghosh, K. N. V. D. Adarsh, T. Base and T. Pradeep, *ACS Nano*, 2021, **15**, 15781–15793.
36 Z.-Y. Wang, M.-Q. Wang, Y.-L. Li, P. Luo, T.-T. Jia, R.-W. Huang, S.-Q. Zang and T. C. W. Mak, *J. Am. Chem. Soc.*, 2018, **140**, 1069–1076.

37 Q. Li, D. Zhou, J. Chai, W. Y. So, T. Cai, M. Li, L. A. Peteanu, O. Chen, M. Cotlet, X. Wendy Gu, H. Zhu and R. Jin, *Nat. Commun.*, 2020, **11**, 2897.

38 T. Imamoto, T. Oshiki, T. Onozawa, T. Kusumoto and K. Sato, *J. Am. Chem. Soc.*, 1990, **112**, 5244–5252.

39 S. Bestgen, O. Fuhr, B. Breitung, V. S. Kiran Chakravadhanula, G. Guthausen, F. Hennrich, W. Yu, M. M. Kappes, P. W. Roesky and D. Fenske, *Chem. Sci.*, 2017, **8**, 2235–2240.

40 M.-C. Brandys and R. J. Puddephatt, *J. Am. Chem. Soc.*, 2002, **124**, 3946–3950.

41 X. Kang, S. Wang and M. Zhu, *Chem. Sci.*, 2018, **9**, 3062–3068.

42 E. Khatun, A. Ghosh, P. Chakraborty, P. Singh, M. Bodiuzzaman, P. Ganesan, G. Natarajan, J. Ghosh, S. K. Pal and T. Pradeep, *Nanoscale*, 2018, **10**, 20033–20042.

43 M. S. Bootharaju, S. Lee, G. Deng, H. Chang, W. Baek and T. Hyeon, *J. Chem. Phys.*, 2021, **155**, 014307.

44 L. Pauling and R. B. Corey, *Nature*, 1953, **171**, 59–61.

45 F. H. Crick, *Nature*, 1952, **170**, 882–883.

46 A. J. Savyasachi, O. Kotova, S. Shanmugaraju, S. J. Bradberry, G. M. Ó'Máille and T. Gunnlaugsson, *Chem*, 2017, **3**, 764–811.

47 M. R. Molla, A. Das and S. Ghosh, *Chem. – Eur. J.*, 2010, **16**, 10084–10093.

48 S. M. Wagalgave, S. D. Padghan, M. D. Burud, M. A. Kobaisi, D. D. La, R. S. Bhosale, S. V. Bhosale and S. V. Bhosale, *Sci. Rep.*, 2019, **9**, 12825.

49 G. D. Pantoș, P. Pengo and J. K. M. Sanders, *Angew. Chem., Int. Ed.*, 2007, **46**, 194–197.

50 M. Al Kobaisi, S. V. Bhosale, K. Latham, A. M. Raynor and S. V. Bhosale, *Chem. Rev.*, 2016, **116**, 11685–11796.

51 X. Q. Liang, Y. Z. Li, Z. Wang, S. S. Zhang, Y. C. Liu, Z. Z. Cao, L. Feng, Z. Y. Gao, Q. W. Xue, C. H. Tung and D. Sun, *Nat. Commun.*, 2021, **12**, 4966.

52 X. Kang and M. Zhu, *Chem. Soc. Rev.*, 2019, **48**, 2422–2457.

53 Z. Luo, X. Yuan, Y. Yu, Q. Zhang, D. T. Leong, J. Y. Lee and J. Xie, *J. Am. Chem. Soc.*, 2012, **134**, 16662–16670.

54 T. Chen, S. Yang, J. Chai, Y. Song, J. Fan, B. Rao, H. Sheng, H. Yu and M. Zhu, *Sci. Adv.*, 2017, **3**, e1700956.